JOURNAL OF GEOPHYSICAL RESEARCH, VOL. 94, NO. C6, PAGES 8125-8134, JUNE 15, 1989

Extracting the Internal Tide From Data: Methods and Observations From the Mixed Layer Dynamics Experiment

MURRAY D. LEVINE AND JAMES G. RICHMAN

College of Oceanography, Oregon State University, Corvallis

Several methods are developed for analyzing data containing a highly variable internal tide. In particular, the methods are aimed at the analysis of moored observations with relatively few measurements in the vertical. The analysis depends upon an "elliptical decomposition" that is a generalization of the familiar "rotary decomposition." The technique is applied to velocity and temperature observations in the upper ocean made during the Mixed Layer Dynamics Experiment (MILDEX) in the northeast Pacific Ocean, about 700 km west of Santa Barbara, California, during October–November 1983. The observed propagation direction and amplitude of the internal tide was highly variable in time. It was anticipated that the wave could be propagating from the continental shelf where it is presumed to be generated. However, most of the time the internal tide appears to be propagating parallel to the coast. This result suggests the importance of density and velocity structure at mesoscale and frontal scale in affecting the propagation of the internal tide.

1. INTRODUCTION

The term baroclinic or internal tide suggests internal wave oscillations that occur with astronomic regularity. Under this presumption, the naive might assume that it is straightforward to determine the behavior of the internal tide and to predict these baroclinic oscillations with the same reliability as the barotropic tide. However, the internal tide is not forced directly by the gravitational attraction of the Sun and Moon, but is generated by the interaction of the barotropic tide with topography [e.g., *Wunsch*, 1975; *Henderschott*, 1981]. Variations in the density and velocity fields near the generator produce variations in the response of the internal tide [e.g., *Baines*, 1982; *Chuang and Wang*, 1981]. Away from the source the internal tide is reflected and refracted by the density and velocity field through which it propagates; space and time variations caused by eddies and fronts may significantly distort the periodicities that are usually associated with tidal oscillations. The result is an internal tide that is highly variable in time and space.

The generation and propagation of the internal tide can be quite complicated, potentially involving nonlinearities that could lead to the creation of internal solitons and even turbulence [e.g., *Pingree et al.*, 1983]. However, it is presumed that in the far field of the generator, say, the continental shelf, there remains a significant part of the flow that is identifiable as a horizontally propagating linear wave.

The purpose of this paper is to present some techniques for analyzing data that contain a highly variable internal tide. The analysis is directed toward experiments with relatively few moored observations, such as a few current meters on a single mooring, a common sampling scheme in physical oceanography. As an example, the techniques are applied to velocity and temperature observations made during the multiinstitutional Mixed Layer Dynamics Experiment (MILDEX). A primary goal is to determine the amplitude and propagation direction of the internal tide as a function of time. With limited observations that do not span the entire water column, it is not possible to remove the barotropic tide using vertical integration nor decompose the signal into baroclinic modes. However, the main features of the internal tide may be estimated using the most robust properties of internal wave dynamics. This analysis could also be a useful precursor to more sophisticated, model-dependent analyses.

The analysis depends on an "elliptical decomposition" to describe an oscillating flow. At a single frequency the hodograph of the horizontal velocity field can be described by an ellipse. It will be shown that any elliptical hodograph can be expressed uniquely as the sum of two other counterrotating elliptical hodographs with a specified ellipticity and orientation of the major axis. This decomposition is a generalization of the familiar "rotary decomposition," where the hodograph is described by two counterrotating, circular hodographs. For an internal wave of a specified frequency, the hodograph is an ellipse with known ellipticity and rotation. Thus elliptical hodographs of a specific ellipticity are a more natural basis to describe internal tide motion than circular hodographs.

The dynamics of the internal tide are reviewed in section 2, providing the motivation for the elliptical decomposition and the analysis methods developed in section 3. The observations are discussed in section 4 and analyzed for internal tide in section 5. Conclusions and summary are presented in sections 6 and 7.

2. THEORY

In order to interpret the observed oscillations we review the theoretical behavior of the internal tide. The linear momentum equations for a Boussineq, rotating, stratified fluid can be writte

$$\frac{\partial u}{\partial t} - fv = -\frac{1}{\rho_0}\frac{\partial p}{\partial x} \tag{1}$$

$$\frac{\partial v}{\partial t} + fu = -\frac{1}{\rho_0}\frac{\partial p}{\partial y} \tag{1'}$$

Paper number 89JC00415.
0148-0227/89/89JC-00415$05.00

$$\frac{\partial w}{\partial t} = -\frac{1}{\rho_0}\frac{\partial p}{\partial z} - \frac{\rho}{\rho_0} g \tag{1''}$$

where (u, v, w) is the wave-induced velocity field and ρ and p are the excess or wave-induced density and pressure fluctuations that remain after the hydrostatic balance has been subtracted [e.g., *Gill*, 1982]. For an incompressible, ideal fluid additional relations are obtained:

$$\frac{\partial u}{\partial x} + \frac{\partial v}{\partial y} + \frac{\partial w}{\partial z} = 0 \tag{1'''}$$

$$\frac{\partial \rho}{\partial t} = \frac{\rho_0 N^2}{g} w \tag{1''''}$$

where

$$N^2 = -\frac{g}{\rho_0}\frac{\partial \bar{\rho}(z)}{\partial z}$$

is the buoyancy frequency and $\rho_0 + \bar{\rho}(z)$ represents the unperturbed density field. There are five equations that can be solved for five unknowns: u, v, w, ρ, and p.

Assume the solution is a wave propagating horizontally at an angle β from the x axis of the form

$$(u, v, w) = \left[\frac{\hat{u}}{\kappa}\frac{\partial \Psi(z)}{\partial z}, \frac{\hat{v}}{\kappa}\frac{\partial \Psi(z)}{\partial z}, \hat{\omega}\Psi(z)\right] e^{i[\kappa(x\cos\beta + y\sin\beta) - \omega t]} \tag{2}$$

where the velocity amplitudes $\hat{u}$, $\hat{v}$, *and* $\hat{w}$ are functions of β, κ (horizontal wave number), and ω (frequency), and the real part of the right-hand side is implied. Using (1) and (2), the following relationships between velocity amplitudes are found:

$$\hat{u} = \left(i\cos\beta - \frac{f}{\omega}\sin\beta\right)\hat{w} \tag{3a}$$

$$\hat{v} = \left(i\sin\beta + \frac{f}{\omega}\cos\beta\right)\hat{w} \tag{3b}$$

and the vertical wave function is defined by

$$\frac{\partial^2 \Psi}{\partial z^2} + \kappa^2\left[\frac{N^2(z) - \omega^2}{\omega^2 - f^2}\right]\Psi = 0 \tag{4}$$

It is convenient to express the velocity field in a horizontal coordinate system rotated at angle β (indicated by primes) so that the propagation direction is aligned with the x' axis (Figure 1). Using (2) and (3), the velocity in the rotated frame of reference becomes

$$(u', v', w') = \left[i\frac{\hat{w}}{\kappa}\frac{\partial \Psi}{\partial z}, \frac{f}{\omega}\frac{\hat{w}}{\kappa}\frac{\partial \Psi}{\partial z}, \hat{w}\Psi\right] e^{i(\kappa x' - \omega t)} \tag{5}$$

Assuming the boundary conditions $\Psi = 0$ at the top and bottom of the ocean, (4) becomes an eigenvalue problem with wave function solutions Ψ_n at wave number κ_n.

The general solution of (5) can then be expressed as the sum of many vertical modes. Assuming that all modes are propagating in the same horizontal direction β, the solution can be written in the form

$$u' = i\Phi_1 e^{i(\phi_1 - \omega t)} + \hat{u}_0 e^{-i\omega t} \tag{6a}$$

$$v' = \frac{f}{\omega}\Phi_1 e^{i(\phi_1 - \omega t)} + \hat{v}_0 e^{-i\omega t} \tag{6b}$$

$$w' = \Phi_2 e^{i(\phi_2 - \omega t)} \tag{6c}$$

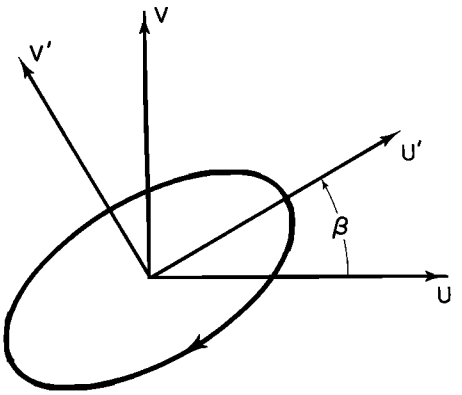

Fig. 1. Hodograph of horizontal velocity of the internal tide. Velocity components u and v are in the east and north direction, respectively. The primed frame is rotated an angle β such that u' is aligned with the propagation direction of the internal tide. The velocity vector rotates clockwise in the northern hemisphere.

where

$$\Phi_1 e^{i\phi_1} = \sum_{n=1}^{\infty} \frac{\hat{w}_n}{\kappa_n}\frac{\partial \Psi_n(z)}{\partial z} e^{i\kappa_n x'}$$

$$\Phi_2 e^{i\phi_2} = \sum_{n=1}^{\infty} \hat{w}_n \Psi_n(z) e^{i\kappa_n x'}$$

The amplitude of the depth-independent barotropic tide is given by constants $\hat{u}_0$ and $\hat{v}_0$; horizontal variation of the tide has been neglected. For simplicity the vertical velocity component of the barotropic tide is neglected, since it is usually much smaller than the vertical velocity due to the internal tide, especially in regions where an internal tide analysis would be attempted.

Each baroclinic mode is conveniently expressed as a hodograph of the velocity vector (Figure 1). Since for internal waves u' and v' are always in quadrature, the hodograph in the horizontal plane is an ellipse with the velocity vector rotating anticyclonic in time (clockwise in the northern hemisphere). The major axis of the ellipse is oriented along the axis of propagation (x' axis), and the ratio of the minor to major axis is given by f/ω. These properties are independent of the modal composition of the wave. By looking at this hodograph alone, it is not possible to determine if the wave is propagating in the $+x'$ or $-x'$ direction. To remove this ambiguity additional information about the vertical velocity field and modal structure is needed.

There is no constraint on the ellipticity or rotation direction of the hodograph of the barotropic tide. Thus the properties of the hodograph of the total velocity including the barotropic tide are not easily predicted.

A description of the hodograph of internal waves in the vertical plane of u' and w' or v' and w' depends critically upon the modal composition. However, for a single mode $\phi_1 = \phi_2$, and u' and w' are in quadrature producing an elliptical hodograph aligned with the x' axis, and v' and w' are in phase forming a straight-line hodograph.

In practice, it is difficult to estimate and remove the barotropic tide from current observations, since the barotropic tide occurs at the same frequency as the internal tide. Often, the barotropic tide is removed as the vertical averaged flow or as the residual flow after decomposing into

vertical modes. However, these techniques require complete sampling over the entire water column with many measurements in the vertical. Lacking this dense vertical sampling, other techniques must be used. Estimation and removal of the barotropic tide may be avoided by considering horizontal velocity differences in the vertical instead of the velocity itself. The horizontal velocity difference between two depths z_1 and z_2 can be written from (6) as

$$\Delta u' = iQ(z_1, z_2)e^{-i\omega t} \tag{7a}$$

$$\Delta v' = (f/\omega)Q(z_1, z_2)e^{-i\omega t} \tag{7b}$$

where

$$Q(z_1, z_2) = \Phi_1(z_1)e^{i\phi_1(z_1)} - \Phi_1(z_2)e^{i\phi_1(z_2)}$$

Since the z dependence of $\Delta u'$ and $\Delta v'$ is the same, the hodograph of the horizontal velocity difference has the same properties as the hodograph of baroclinic velocity without the additional complication of the barotropic tide. Velocity differences are used rather than derivatives of velocity to permit direct application to observations.

In the next section these theoretical relationships are used to develop techniques for internal tide analysis.

3. Analysis Methods

The first step in analyzing the semidiurnal internal tide is to extract the signal at tidal frequency. The technique of complex demodulation is applied independently to each component of velocity to determine the amplitude and phase of the tide. Since the observed internal tide is not steady, the analysis is done over short segments of data to produce a best fit amplitude and phase as a function of time.

The second part of the analysis attempts to select the portion of the demodulated series that is consistent with theoretical expectations of the internal tide developed in section 2. Two methods are developed for estimating the propagation direction and amplitude of the tide from the observations. Each method uses different criteria in determining the best fit: method 1 uses the ellipticity and polarization of the hodograph of horizontal velocity difference between two depths, and method 2 uses the phase relation between the horizontal and vertical velocity. The advantage of method 1 is that no assumption of the vertical modal structure is necessary. In method 1 the velocity differences between vertically separated observations are used as a means of eliminating the barotropic tide. In method 2 some assumption about the modal composition must be made to relate the horizontal and vertical velocity. Both methods are discussed in this section and applied to the data in section 5.

3.1. *Complex Demodulation*

Complex demodulation is a technique used to estimate from data the amplitude and phase of a harmonic component at a given frequency [*Koopmans*, 1974]. The procedure consists of multiplying the real time series $u(t)$ by a complex exponential $e^{i\omega_0 t}$. The complex amplitude $\tilde{u}$ of the resulting series near zero frequency is the same as the complex amplitude of $u(t)$ near frequency ω_0. Hence applying a narrow-band, low-pass filter to $u(t)e^{i\omega_0 t}$ yields the complex amplitude at frequency ω_0. In this case the frequency ω_0 was chosen to be $2\pi/12.5$ hours; this frequency is very close to the M_2 tide (12.4-hour period) and can be accurately applied to hourly data. The filtering was accomplished by using a "boxcar" window in time of length 25 hours and integrating:

$$\tilde{u}(t_m) = \frac{1}{25}\sum_{(n=-12)}^{12} e^{in\omega_0}u(t_{n+m}) \tag{8}$$

This short filter length was chosen because the data measured during MILDEX varied rapidly in time; frequency resolution was sacrificed in favor of temporal resolution. Values of $\tilde{u}$ can then be estimated at each hour and represent the complex amplitude at the tidal frequency based on an average over two tidal periods.

The statistical significance of the estimate of $\tilde{u}$ is based on how well the complex demodulated signal represents the total variability. After determining $\tilde{u}$, the data can be represented by

$$u(t_m) = Re\{\tilde{u}(t_m)e^{-i\omega_0 t_m}\} + Z(t_m) \tag{9}$$

where $Re\{\ \}$ is the real part and Z is the residual. The demodulation was also performed independently for velocity components v and w as well.

An F statistic can be formed by the ratio of mean-square signal to mean-square residual:

$$F_{2,22}(t_m) = \frac{\frac{1}{2}|\tilde{u}(t_m)|^2}{\frac{1}{22}\sum_{n=-12}^{12} Z^2(t_{m+n})} \tag{10}$$

with 2 degrees of freedom in the numerator and 22 in the denominator. For the estimated value of $\tilde{u}$ to be significant at the 95% significance level the value of F must be greater than 3.44; if F was less than 3.44, then no significant estimate of the tide is possible. Using this screening criterion only tidal signals that represent a significant part of the total variance are analyzed.

3.2. *Methods for Extracting the Internal Tide*

3.2.1. *Method one.* This method uses the ellipticity and rotation direction of the hodograph of the horizontal velocity difference as criteria for determining the amplitude and propagation direction of the tide. For a horizontally propagating internal tide from a single source the major axes of the ellipses are oriented in the propagation direction, the ratios of the minor-to-major axis are fixed at $r = f/\omega_0$ (section 2) and the horizontal velocity vector rotates anticyclonic in time. This is also true for the velocity difference between any two depths and is independent of the modal baroclinic composition. This behavior provides the motivation for elliptical decomposition.

It is possible to express any hodograph as the sum of two counterrotating ellipses with both major axes oriented at a given angle β and with the ratios of the major-to-minor axis of both ellipses set to r. In one of the ellipses the vector rotates clockwise, in the other the vector rotates anticlockwise. The clockwise component is consistent with an internal wave in the northern hemisphere; the anticlockwise component is considered "noise," since it cannot be explained by simple internal wave dynamics. The decomposition is unique for any given β and r. This decomposition is a generalization of the standard rotary decomposition where the hodograph is expressed as the sum of two counterrotat-

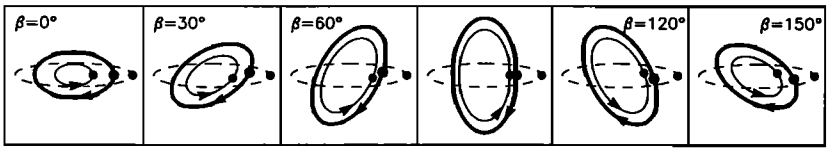

Fig. 2. Example of elliptical decomposition, A clockwise-rotating elliptical hodograph with arbitrary ellipticity (dashed line) is decomposed into a clockwise-rotating hodograph (heavy solid line) and an anticlockwise hodograph (light solid line) with ellipticity determined by internal wave kinematic constraints for various values of orientation angle β. The dots indicate the relative position of the velocity vector at a given time.

ing circles (degenerate ellipses) and is analogous to determining the Stokes parameters for the polarization of a beam of electromagnetic radiation (c.f. *McMasters* [1954] for a review of applications of Stokes parameters). Ellipses are a more natural basis than circles in describing internal waves at frequencies greater than inertial.

The general procedure for decomposing any periodic, two-dimensional velocity of the form

$$u = u_1 \cos \omega t + u_2 \sin \omega t \tag{11a}$$

$$v = v_1 \cos \omega t + v_2 \sin \omega t \tag{11b}$$

into two counterrotating ellipses is as follows. The velocity of the clockwise- and anticlockwise-rotating vector can be represented by

$$u_c' = C \cos (\omega t + \varepsilon) \tag{12a}$$

$$v_c' = rC \cos (\omega t + \pi/2 + \varepsilon) \tag{12b}$$

$$u_a' = A \cos (\omega t + \eta) \tag{12c}$$

$$v_a' = rA \cos (\omega t - \pi/2 + \eta) \tag{12d}$$

respectively, where the u' axis is aligned with the major axis of the ellipse at an angle β. The major axes of the clockwise and anticlockwise ellipses are 2C and 2A, respectively, and ε and η are absolute phases. After equating the total velocity (u, v) to the sum of the clockwise (u_c', v_c') and anticlockwise (u_a', v_a') rotating components in the rotated frame, the following transformation equations result:

$$\begin{pmatrix} \cos\beta & -r\sin\beta & \cos\beta & r\sin\beta \\ -r\sin\beta & -\cos\beta & r\sin\beta & -\cos\beta \\ \sin\beta & r\cos\beta & \sin\beta & -r\cos\beta \\ r\cos\beta & -\sin\beta & r\cos\beta & -\sin\beta \end{pmatrix} \begin{pmatrix} W \\ X \\ Y \\ Z \end{pmatrix} = \begin{pmatrix} u_1 \\ u_2 \\ v_1 \\ v_2 \end{pmatrix} \tag{13}$$

where the unknowns are $W = A \cos \eta$, $X = A \sin \eta$, $Y = C \cos \varepsilon$, and $Z = C \sin \varepsilon$. Hence any velocity (specified by u_1, u_2, v_1, v_2) (11) can be decomposed into a clockwise and anticlockwise component (specified by C, ε, A, η) (12) for a given orientation angle β and ratio r. An example of the decomposition of a sample hodograph for various values of β is shown in Figure 2.

This procedure for elliptical decomposition is applied to the horizontal velocity difference data which has already been complex demodulated at tidal frequency. The value of r is fixed at f/ω_0. For a specified β, at depth z_m and time t, estimates of the amplitudes A and C can be calculated using (13). A measure R^2 of the overall goodness of fit of the observed hodograph to the clockwise-rotating hodograph that is consistent with the internal tide in the northern hemisphere is defined in analogy to a noise-to-signal ratio by

$$R^2(\beta, t) = \frac{1}{M} \sum_{m=1}^{M} \left(\frac{A(z_m; \beta, t)}{C(z_m; \beta, t)} \right)^2 \tag{14}$$

The best fit orientation angle β_B is defined to be, where R^2 is a minimum with respect to β. If there were no anticlockwise component at some angle β at all depths, then $R^2 = 0$. The value of R^2 at the best fit orientation angle gives an indication of the goodness of the fit; a value less than 1 indicates that there is more internal tidal signal than noise on average. The results of this method are independent of the specific modal composition of the tide; the method selects the orientation angle that yields the optimum set of clockwise-rotating hodographs consistent with the theoretically determined ellipticity.

It is also useful to estimate the uncertainty in the best fit value of β determined by a minimum in R^2. Upper and lower bounds, β_U and β_L, of the best fit angle β_B are chosen such that

$$R(\beta_L) = R(\beta_U) = R(\beta_B) + \sigma_R \tag{15}$$

where σ_R is the standard deviation of R^2 (Figure 3). For small σ_R, β_U, and β_L are very near β_B. If σ_R is too large, there will not be a solution for β_L and β_U; in this case no significant estimate of β_B can be made.

One of the deficiencies of this method is that not all of the possible information from internal wave dynamics has been used, in particular relationships between the vertical and horizontal velocity. To include w, the vertical velocity, into the analysis requires assumptions about the modal structure. A simple way of incorporating w into the analysis is demonstrated in method two.

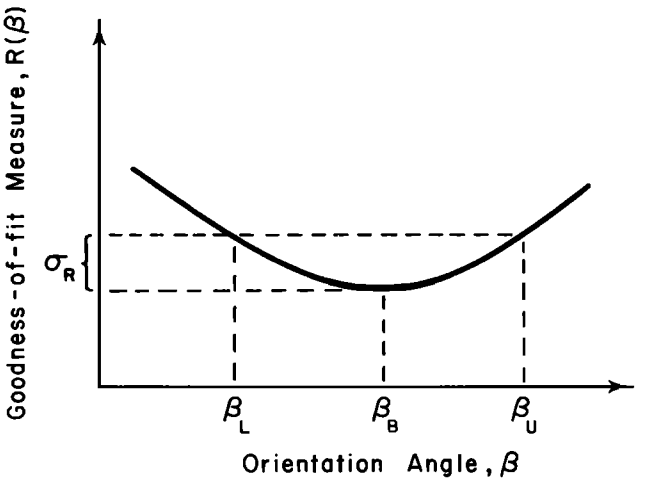

Fig. 3. Schematic of the goodness-of-fit measure R as a function of β. The best fit value β_B occurs at the minimum of R; lower and upper bounds (β_L and β_U, respectively) mark the values of β within one standard deviation of R.

3.2.2. *Method two.* The second method uses the phase relationship between the vertical and horizontal velocity to determine the orientation angle β. This method does require assumptions about the modal composition and the barotropic tide that are not needed in method one. If one assumes that a single mode dominates at a given depth, then the phase between u_c' and w is either $-\pi/2$ or $+\pi/2$ (section 2), where u_c' is the clockwise velocity component along the major axis at propagation angle β. It is not required that the same mode dominate at all the depths where simultaneous observations of u, v, and w are available. If the observed value of w at depth z_m is expressed as

$$w(z_m) = W(z_m) \cos [\omega t + \gamma(z_m)] \tag{16}$$

then a measure of the average phase angle between w and u_c' can be defined by

$$\Delta(\beta, t) = \frac{1}{M} \sum_{m=1}^{M} |\gamma(z_m; t) - \varepsilon(z_m; \beta, t)| \tag{17}$$

where ε is determined from the observed horizontal velocity using the ellipse decomposition for a given β (equation (13)), and the phase γ is estimated directly from the complex demodulated vertical velocity and is not a function of β. The best fit value of β is chosen when Δ is nearest $\pi/2$.

This method has another disadvantage besides having to assume that one mode dominates at each depth: the barotropic tide cannot be easily removed. The vertical velocity is undoubtedly dominated by the internal tide, but the presence of a significant barotropic tide could affect the horizontal velocity. This problem was eliminated in method one by using velocity differences. However, in method two the barotropic tide must be assumed small or be removed by some other method from the horizontal velocity signal.

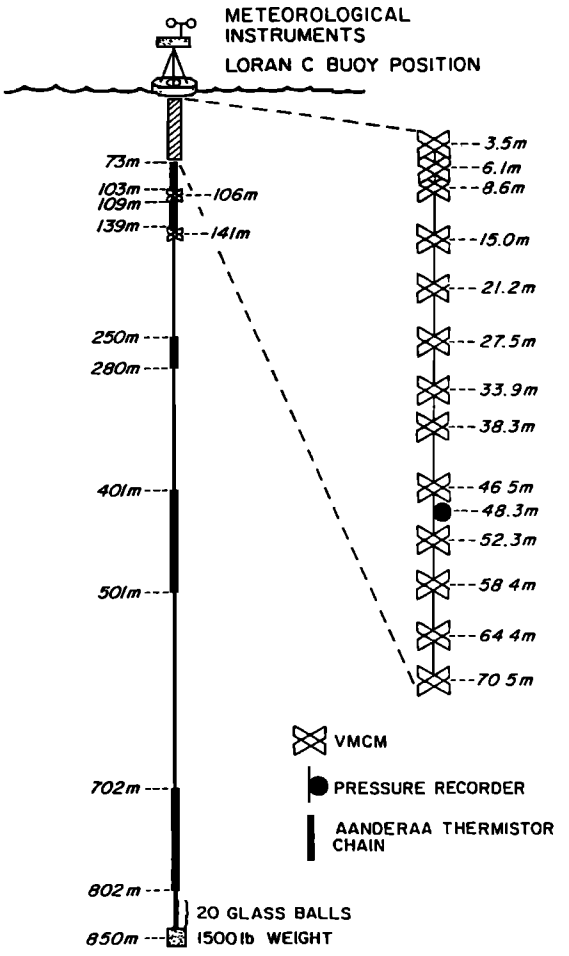

Fig. 4. Schematic diagram of the Current Meter Drifter.

4. Observations

MILDEX took place in the northeastern Pacific Ocean about 700 km west of Santa Barbara, California, during October–November 1983. The data for this study come from a free-floating string of instruments called the Current Meter Drifter (CMD) (Figure 4). The water depth was approximately 4700 m in the region. The CMD consisted of a toroid buoy that supported 15 Vector-Measuring Current Meters (VMCMs) from 3 to 141 m and 4 Aanderaa thermistor chains from 70 to 800 m [*Paduan et al.*, 1988; *Levine et al.*, 1984]. The two upper thermistor chains were 30 m in length; the two lower chains were 100 m in length. Each had 11 thermistors distributed equally along its length. Data were recorded every 5 min for the chains and every 2 min for the VMCMs. The toroid buoy also contained a suite of meteorological sensors, a Loran-C receiver and a satellite transmitter. An analysis of the heat and momentum budgets using data from the CMD is given by *Paduan et al.* [1988].

The CMD was deployed on October 25 near 33° 51'N, 126° 42'W; recovery occurred 19 days later about 80 km to the northeast (Figure 5). The average drift speed was about 0.06 m/s. During the experiment, the upper 50 m were weakly stratified with little current shear [*Paduan et al.*, 1988]. Since the CMD drifted, the current meters measured the relative velocity that is not representative of either a Lagrangian or Eulerian frame of reference. The velocity of the CMD itself was determined from hourly positions measured by Loran-C. The CMD velocity was then added to each current meter observation to produce a time series of absolute current. Although the position data is somewhat noisy and required editing and filtering, the CMD velocity was probably determined adequately enough to resolve tidal frequencies.

For this analysis horizontal velocity records from three current meters at 27, 70, and 141 m were used. The 12 other current meters were not explicitly included in the analysis since the instruments shallower than 65 m did not add significantly independent information about the tidal oscillations and the instrument at 105 m failed halfway through the experiment. The data from 27 m were representative of the velocity in the mixed layer which contained little vertical shear at tidal frequency; the record at 141 m was below the maximum depth of the seasonal pycnocline for this region. Sample time series are shown in Figure 6.

Vertical velocity was calculated from the vertical displacement of isotherms (Figure 6). Isotherm depths were estimated from the thermistor chain records by assuming a linear temperature gradient between adjacent thermistors. While all the deeper thermistor chains measured significant tidal signals, a single isotherm could not be tracked throughout the experiment. The isotherm with a mean depth of 85 m from uppermost chain was the most useful to include in the joint analysis with the current records.

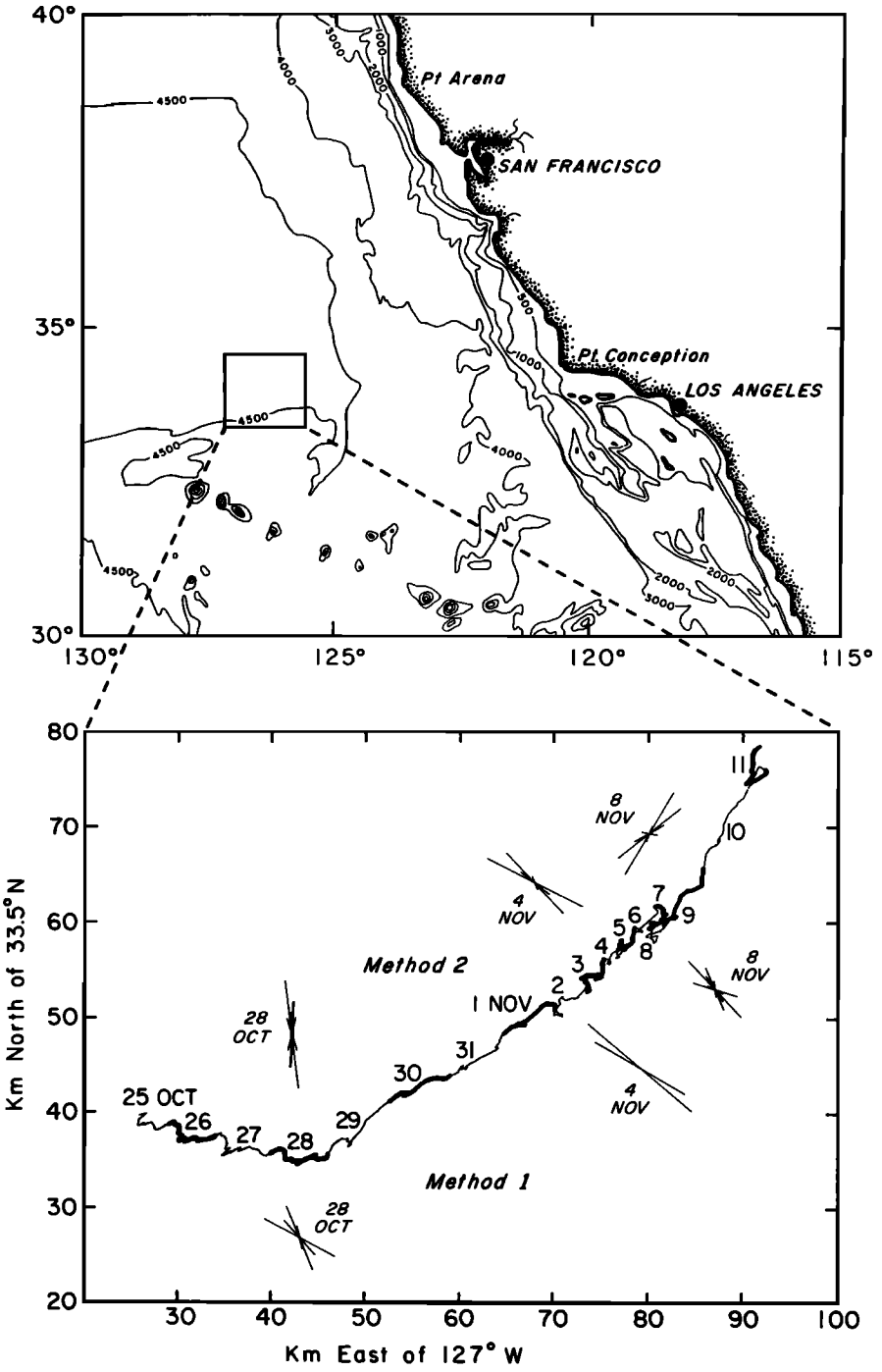

Fig. 5. Map showing the location of the MILDEX site (top). The track of the Current Meter Drifter is shown along with propagation direction of the internal tide for selected days determined by methods 1 and 2 (bottom).

5. Application of Analysis Methods to Observations

The MILDEX observations used in this analysis are hourly values of horizontal velocity at 27, 70, and 141 m and vertical velocity at 85 m. These data are combined to extract the tidal signal using the two methods presented in section 3.

The first step in the tidal analysis is to estimate the signal in the semidiurnal tidal band using complex demodulation. Examples of the time series of amplitude and phase for the u component of absolute velocity are shown in Figure 7. The variability of the amplitude of the complex demodulated series appears reasonable when compared visually with the velocity time series (Figure 6). The modulation of the amplitude in the semidiurnal tidal band is often rapid. Relatively large-amplitude events occur for only 3 or 4 tidal cycles, barely long enough to be confident that the signal is of tidal origin. The amplitudes at 27 and 141 m are not correlated through the first half of the experiment; however, in the second half the time series of amplitudes appear to track each other more closely. Patterns are difficult to detect and interpret especially considering that the v component (not shown) is similarly confused. The complexity of the

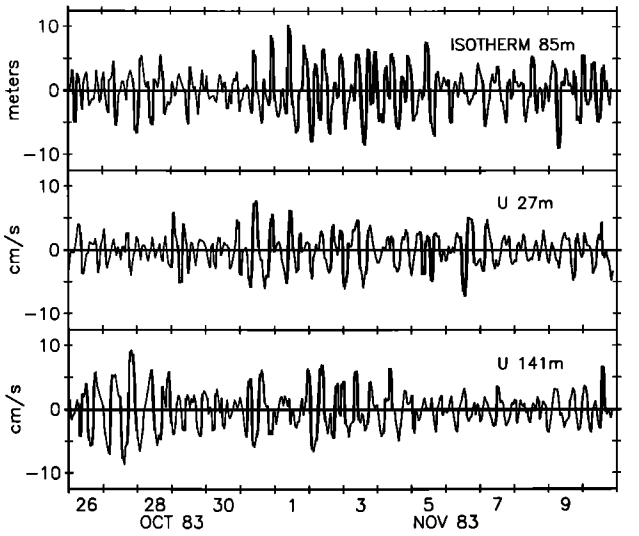

Fig. 6. Time series of the isotherm centered at 85 m and the u velocity component at 27 and 141 m.

time series of amplitude and phase prevented a straightforward determination of the amplitude and propagation direction of the wave signal consistent with theory and hence acted as motivation for the procedures developed in section 3.

Using the complex demodulated series as input, the best fit horizontal direction of propagation is shown in Figure 8 as determined by methods 1 and 2 (section 3). Since these methods only determine the orientation of the axis of propagation, there is a 180° ambiguity in the actual propagation direction. For example, a propagation angle of 90° implies either northward or southward propagation. The shaded region indicates the best fit by method 1, which was determined using three horizontal velocity differences in the vertical between 27 and 70 m, 70 and 141 m, and 27 and 141 m. The width of the shading is a measure of the uncertainty in estimating a best fit (equation (15)). Since velocity differences are used, these results are the same using either absolute or relative velocities. Although the motivation for

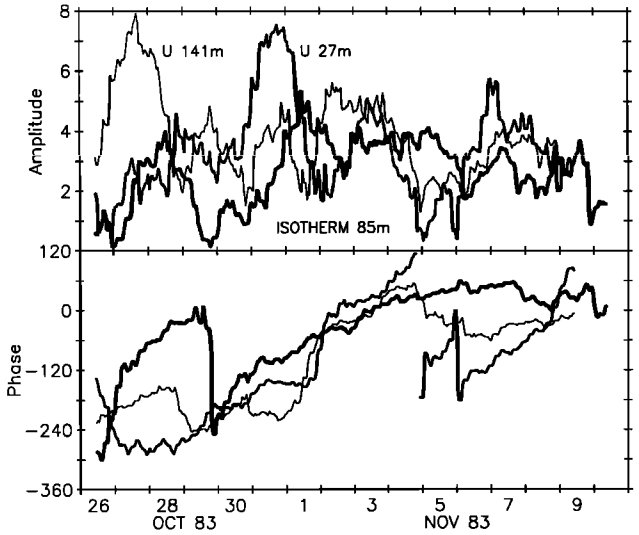

Fig. 7. Amplitude and phase of the semidiurnal frequency component determined by complex demodulation of the time series shown in Figure 6.

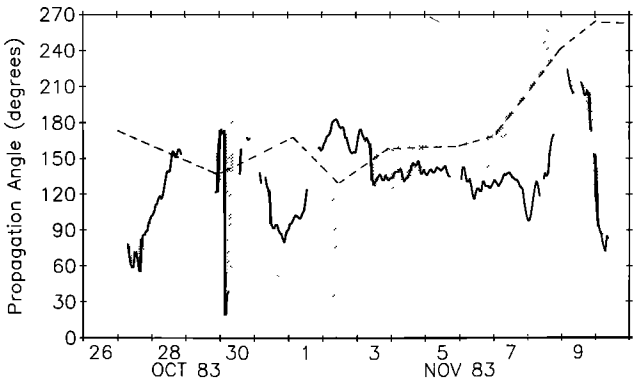

Fig. 8. Propagation angle of the internal tide determined by method 1 (shaded area) and method 2 (solid line). Results of analysis by *Williams* [1986] are shown for comparison (dashed line).

using velocity differences was to eliminate contamination by the barotropic tide, it also eliminates errors made in transforming the measured relative velocity into an absolute velocity.

The propagation angle from method 2, plotted as a solid line, was determined by forcing the absolute phase difference between the vertical velocity at 85 m and the major-axis component of the horizontal velocity at 70 m to be $\pi/2$. It is assumed that 70 and 85 m are close enough so that the vertical and horizontal velocities can be regarded as being at the same depth. For the first or second baroclinic modes of horizontal velocity with zero crossings at 1370 m and 215 m, respectively, the difference in depth is probably negligible. Since the current meter at 106 m and the thermistor chain from 109 to 139 m did not function, there is only one reliable estimate of vertical and horizontal velocity from the same location. Thus the propagation angle, as determined from (17) with $M = 1$, has a unique answer. If more data were available ($M > 1$), then a least squares fit would provide an estimate of the uncertainty in the angle as was done in method 1. The fit using method 2 was tried using both the absolute and the relative velocity at 70 m. Recall that the presence of significant barotropic tide in the horizontal velocity would contaminate the results obtained using method 2. In these data the best fit propagation angles estimated from either absolute or relative velocities were close most of the time. It is assumed that the CMD tended to drift with the barotropic current field, since drag on the drifter was distributed over 1000 m. Hence the CMD would tend to oscillate with the barotropic tidal currents, and the current meter would measure primarily the baroclinic tide. Therefore the results of method 2 that were calculated from the relative velocity will be used throughout the paper.

The propagation angle determined by either method is quite variable in time. The relatively stable periods, for example, between October 27–28 and November 3–6 are short. The results from the two methods agree fairly well (better than ±45°) during these stable periods, and the overall character of the two plots is similar. However, there are times when there are significant differences of 90°, such as November 8. The period from October 29 to November 2 is especially confused; during this time many properties of the large-scale flow also changed, as though the CMD had drifted through a mesoscale feature [*Paduan et al.*, 1988].

Once the best fit angle is determined, the data ellipse can be decomposed uniquely into a clockwise and anticlockwise

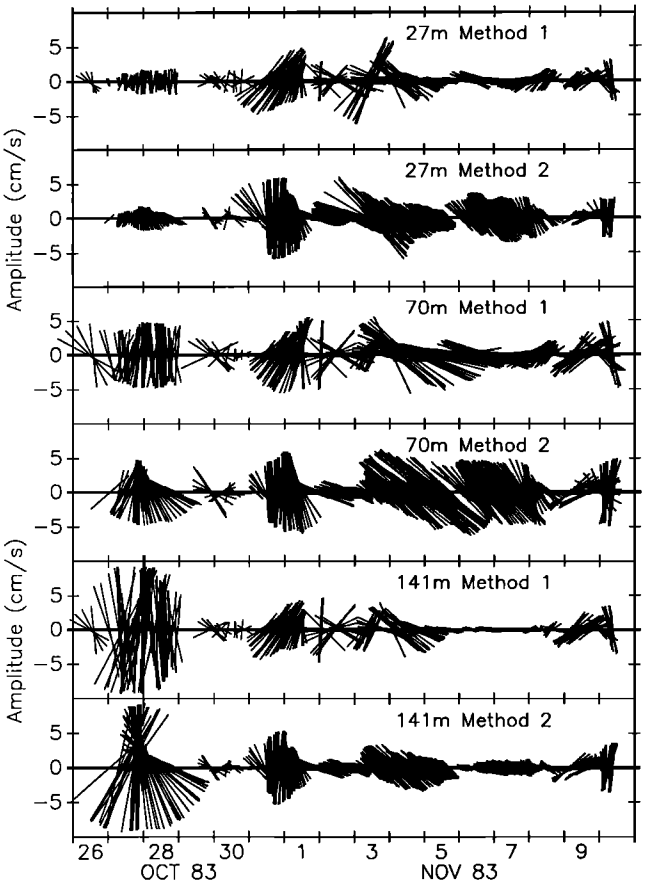

Fig. 9. Time series of best fit clockwise-rotating horizontal velocity hodographs of data from 27, 70, and 141 m by methods 1 and 2. Each line represents the major axis of the hodograph; the length is proportional to the amplitude and the angle indicates the orientation of the ellipse.

rotating hodograph with ellipticity of f/ω_0. The clockwise rotating ellipse is the one consistent with the internal tide, the anticlockwise-rotating ellipse is the "noise." The major axis of the clockwise-rotating ellipse at the best fit propagation angle are shown in Figure 9 for both methods. The length of the line is proportional to the magnitude of the u' velocity component and the angle of the line indicates the propagation direction. Recall that the direction of propagation is ambiguous; the wave may be propagating in either direction along the major axis. The two methods give comparable results much of the time considering the overall large variability of the tide.

Another display of the best fit internal tidal velocity is shown in Figure 10. This figure shows the u' velocity amplitude of the best fit clockwise-rotating internal tidal ellipse as a function of time by method 1. The u' component of the anticlockwise rotating ellipse that does not fit the model of a horizontally propagating internal wave is also shown in the figure. Much of the time the clockwise rotating ellipse dominates the signal at most depths. All these presentations show the large amount of variability and complexity of the internal tide signal. The results from method 2 are similar and therefore are not shown.

A display of the horizontal velocity hodographs themselves is shown in Figure 11 for selected times. On October 28, 0100-hours, both methods choose nearly the same propagation angle. Recall that the best fit angle as found by both methods is not simply based on the orientation of the major axis of the data hodograph, but uses phase information between velocity components as well. The ellipse at 141 m is virtually circular; hence the propagation direction cannot be determined from the shape of the hodograph alone. However, the two independent methods picked nearly the same propagation direction, giving some confidence that the result is valid. Note that the clockwise rotating tide at 27 m is nearly 180° out of phase with both 70 and 141 m, indicating a zero crossing near the depth of the mixed layer at 50 m, which suggests the presence of a mode 4 or greater internal tide. On November 3, 2100 hours, the agreement between methods is again good. In contrast to October 28 the amplitude and phase of the modeled clockwise tide is nearly constant with depth. On November 4, 1700 hours, the phase of the best fit tide is nearly consistent with depth, but there is significant shear between instruments. On November 8, 0000 the two methods do not compare well; the best fit propagation estimates are nearly 90° apart. Note also that the vertical structure changes significantly in time; this is another reason why the fitting of a modal model is not practical.

The propagation direction as determined by both method 1 and 2 are plotted for selected days on the drift track (Figure 5). Each cluster of lines represents a histogram of the ellipse orientation for a given day, in analogy to meteorologists' wind roses. The length of the line is proportional to the fraction of time the ellipse was oriented in that direction for that day. On October 28 and November 4 the directions estimated from both methods are reasonably consistent; the

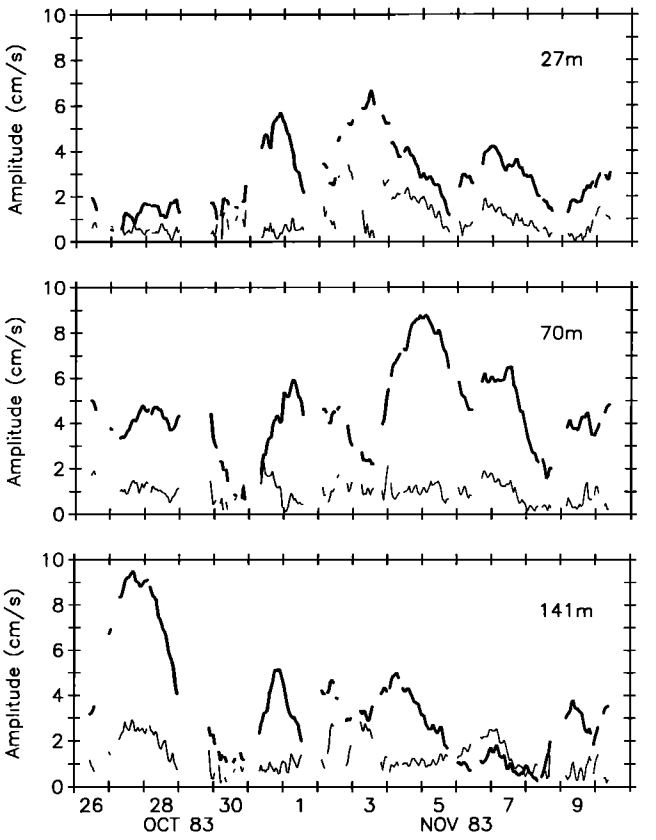

Fig. 10. Time series of the major axis amplitude of the clockwise (heavy line) and anticlockwise (light line) components at the best fit value of β for data from 27, 70, and 141 m.

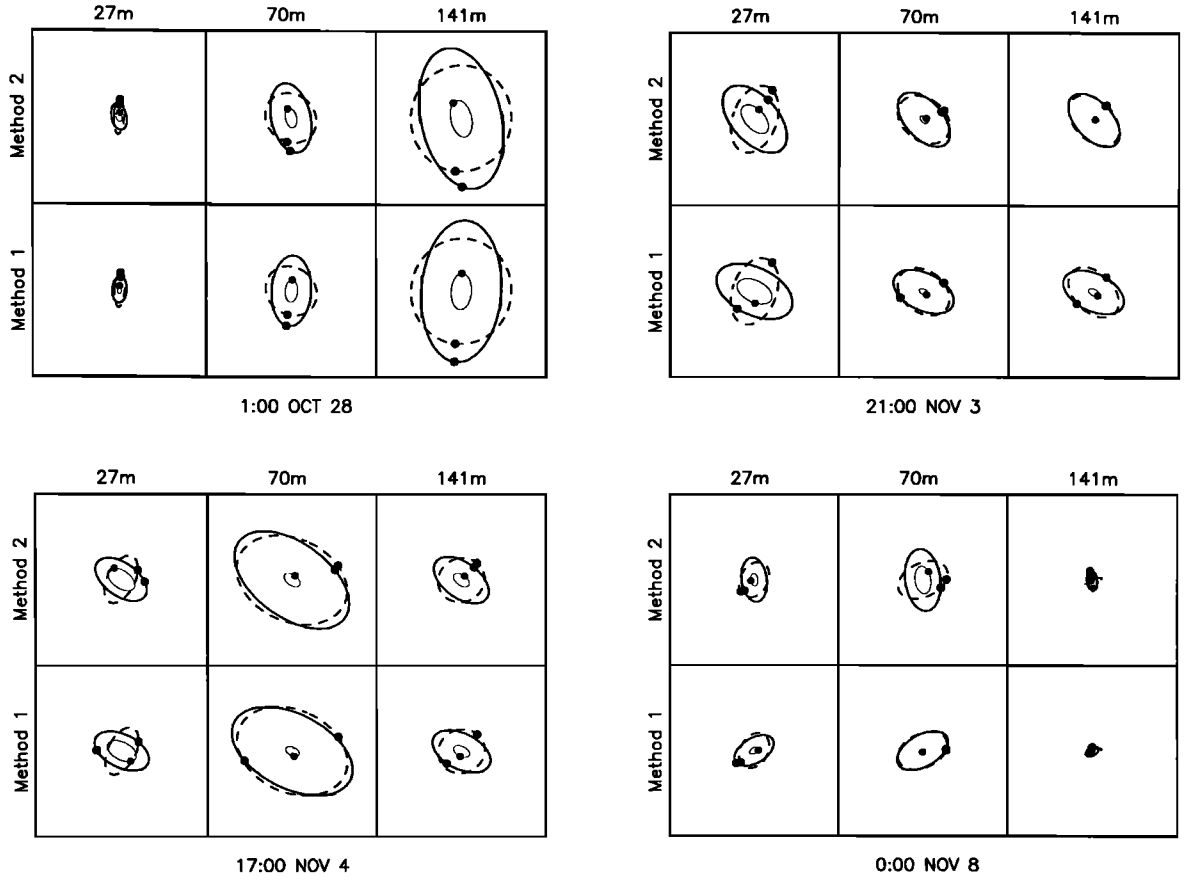

Fig. 11. Elliptical decomposition of the observed hodographs (dashed lines) for selected times using both methods 1 and 2. The clockwise-rotating component is shown as a heavy line and the anticlockwise-rotation component is shown as a light line. The dots indicate the phase of velocity vectors at a given time.

propagation direction is nearly parallel to the California coast. The results for November 8 are shown as an example of a time when the methods do not give similar results.

6. Discussion

Theories of generation [e.g., *Rattray et al.*, 1969; *Baines*, 1982] suggest that the internal tide would propagate away from the shelf in a direction normal to the topography. For the most part during MILDEX, the estimated propagation direction is more often oriented parallel to the coast (Figures 5 and 8). A similar unexpected conclusion was reached independently by *Williams* [1986] using horizontal velocity observations made during MILDEX from RV *FLIP* with an acoustic Doppler sonar. Using a principal axis method, he found the propagation angle to be about 150° from October 27 to November 8 (Figure 8). After November 8 both the CMD and *FLIP* data indicated a rapid change in propagation angle with time. *FLIP* and the CMD were always within 60 km of each other during the experiment, too far to expect high coherence in the internal tidal band, but close enough to expect similar amplitude and propagation direction of the internal tide. Besides the horizontal separation, the two data sets are concentrated over different depth ranges. The CMD analysis is limited to data shallower than 141 m, while the acoustic Doppler sonar data is from 100 to 1000 m.

How can the observed propagation direction be rationalized with generation theories of the internal tide? One possibility is that the internal tide is generated from the continental shelves, but is severely refracted by the mesoscale structure [e.g., *Olbers*, 1981; *Stabeno*, 1982]. Evidence during MILDEX [*Paduan et al.*, 1988; *Baumann et al.*, 1985] and other experiments [*Simpson et al.*, 1984] suggests that significant mesoscale features may be present. Another possibility is that the assumption of a single plane tidal wave at MILDEX may be wrong. Waves radiating from different regions of the coast could result in a complicated wave pattern that would be impossible to sort out with the limited observations available. The plausibility of either of these scenarios requires further study.

The observed large temporal variability of the amplitude of the internal tide was anticipated. A common feature in observations of internal tide has been its high degree of temporal variability. The same factors responsible for the variability of the propagation direction could cause the variability of wave amplitude. A careful analysis by *deWitt et al.* [1986] claimed to resolve the vertical beamlike structure of the internal tide near a topographic generator that was consistent with linear theory. However, even relatively near the generator, they found the signal varied markedly in time apparently due to variability in the mesoscale density and velocity structure between the generator and the observation sites. Relatively small shifts in the position of the beams can cause large fluctuations in the signal strengths at given depths. Since MILDEX was even farther from the generator, it is then not surprising that the signal was highly modulated in time. If waves have arrived from more than

one direction, the possibility for a more complicated signal is increased.

7. Conclusion

In order to extract the semidiurnal internal tidal signal from moored velocity observations with limited vertical resolution, the method of elliptical decomposition was developed. Any horizontal velocity vector oscillating at a single frequency describes an elliptical hodograph. This hodograph can be expressed uniquely as the sum of two counterrotating ellipses with specified ellipticity and major axis orientation. Elliptical decomposition is a generalization of rotary decomposition.

The horizontal velocity vector of a linear, horizontally propagating internal wave traces an ellipse with ellipticity f/ω. The major axis is aligned with the direction of propagation, and the vector rotates in an anticyclonic direction (clockwise in the northern hemisphere). Therefore when a signal is elliptically decomposed, the anticyclonic component is consistent with internal wave kinematics while the cyclonic component is not.

One method of estimating the internal tidal signal for a given ellipticity (f/ω) is to find the propagation direction (ellipse orientation) that maximizes the ratio of the signal (anticyclonic component) to the noise (cyclonic component) at all depths simultaneously. This assumes that the internal tide can be represented locally as a plane wave propagating horizontally from a single direction. No assumptions about the vertical modal structure need to be made. The contamination of the internal tide by the barotropic tide is eliminated by using velocity differences between depths rather than velocity itself. This method is especially useful when the distribution of observations in the vertical is inadequate to describe the barotropic tide.

A second method for determining the properties of the internal tide is presented that combines the vertical and horizontal velocity. The criterion of choosing the propagation angle is that the absolute phase difference between the vertical velocity and the major axis component of the horizontal velocity is $\pi/2$. The propagation angle is the angle that fits this phase relation best for all the data. While still a useful method, the presence of a barotropic tide and complex vertical modal structure could contaminate the results of this procedure.

These methods were applied to observations made in the northeast Pacific during MILDEX in Fall 1983. Time series of velocity measurements from a single vertical array of instruments in the upper ocean. The amplitude and phase of the tidal component varied rapidly in time. Using measurements of horizontal velocity from 27, 70, and 141 m, and vertical velocity from 85 m, estimates of the best fit propagation angle were made. While the estimates are somewhat erratic, it appears that most of the time the internal tide is not propagating from the coast but rather parallel to it. The general result is consistent with independent data from MILDEX as analyzed by *Williams* [1986] and *Pinkel et al.* [1987]. If the internal tide is generated at the continental shelf, then this suggests that the wave is significantly refracted by mesoscale and frontal features that may be present between the shelf and the MILDEX site. Waves arriving simultaneously from different regions of the coast would also contaminate the analysis.

The behavior of the internal tide is far from regular and predictable. Significant variation in time and space suggest the importance of mesoscale and frontal-scale density and velocity structure in affecting internal tide propagation. The plausibility of this suggestion awaits further investigation.

Acknowledgments. We thank Russ Davis, Lloyd Regier, and Roland deSzoeke for their help in planning, preparing and deploying the Drifter. This research was supported by the Office of Naval Research under contracts N00014-76-C-0197, N00014-84-C-0128, and N00014-87-K-0009.

References

Baines, P. G., On internal tide generation models, *Deep Sea Res.*, *29*, 307–338, 1982.

Baumann, R. J., L. M. deWitt, C. A. Paulson, J. V. Paduan, and J. D. Wagner, Towed thermistor chain observations during MILDEX, *Ref. 85-12*, 135 pp., Coll. of Oceanogr., Oreg. State Univ., Corvallis, 1985.

Chuang, W.-S., and D.-P. Wang, Effects of density front on the generation and propagation of internal tides, *J. Phys. Oceanogr.*, *11*, 1357–1374, 1981.

DeWitt, L. M., M. D. Levine, C. A. Paulson, and W. V. Burt, Semidiurnal internal tide in JASIN: Observations and simulations, *J. Geophys. Res.*, *91*, 2581–2592, 1986.

Gill, A. E., *Atmosphere-Ocean Dynamics*, Academic, San Diego, Calif., 1982.

Hendershott, M. C., Long waves and ocean tides, in *Evolution of Physical Oceanography*, edited by B. A. Warren and C. Wunsch, pp. 292–341, MIT Press, Cambridge, Mass., 1981.

Koopmans, L. H., The spectral analysis of time series, in *Probability and Mathematical Statistics*, Academic, San Diego, Calif., 1974.

Levine, M. D., S. R. Gard, and J. Simpkins, Thermistor chain observations during MILDEX, *Ref. 84-9*, 159 pp., Coll. of Oceanogr., Oreg. State Univ., Corvallis, 1984.

McMaster, W. H., Polarization and the Stokes parameters, *Am. J. Phys.*, *22*, 351–362, 1954.

Olbers, D. J., A formal theory of internal wave scattering with applications to ocean fronts, *J. Phys. Oceanogr.*, *11*, 1078–1099, 1981.

Paduan, J. D., R. A. deSzoeke, and J. G. Richman, Balances of heat and momentum at 33.5°N, 127°W in the upper ocean during the Mixed Layer Dynamics Experiment, *J. Geophys. Res.*, *93*, 8147–8160, 1988.

Pingree, R. D., D. K. Griffiths, and G. T. Mardell, The structure of the internal tide at the Celtic Sea shelf break, *J. Mar. Biol. Assoc. UK.*, *64*, 99–113, 1983.

Pinkel, R., A. Plueddemann, and R. Williams, Internal wave observations from *FLIP* in MILDEX, *J. Phys. Oceanogr.*, *17*, 1737–1757, 1987.

Rattray, M., Jr., J. Dworski, and P. Kovala, Generation of long internal waves at the continental slope, *Deep Sea Res.*, *16*, 179–195, 1969.

Simpson, J. J., T. D. Dickey, and C. J. Koblinsky, An offshore eddy in the California Current System, I, Interior dynamics, *Prog. Oceanogr.*, *13*, 5–49, 1984.

Stabeno, P. J., The reflection, transmission and scattering of internal waves at ocean fronts, Ph.D. thesis, Oregon State Univ., Corvallis, 1982.

Williams, R. G., The internal tide off southern California, *SIO Reference 86-1*, Mar. Phys. Lab. of the Scripps Inst. of Oceanogr., Univ. of Calif., San Diego, 1986.

Wunsch, C., Internal tides in the ocean, *Rev. Geophys.*, *13*, 167–182, 1975.

M. D. Levine and J. G. Richman, College of Oceanography, Oregon State University, Oceanography Administration Building 104, Corvallis, OR 97331.

(Received August 12, 1988;
revised February 13, 1989;
accepted November 9, 1988.)